

Bio-Inspired Optoelectronic Neuromorphic Device Based on 2D vdW Ferroelectric Heterostructure for Nonlinearly Preprocessing Visual Information and Convolutional Operation

Feng Guo, Weng Fu Io, Zhaoying Dang, Yuqian Zhao, Sin-Yi Pang, Yifei Zhao, Xinyue Lao, and Jianhua Hao*

The human visual system provides important inspiration for designing energy-efficient and sophisticated artificial visual systems. However, integrating nonlinear preprocessing visual information and convolutional operations analogous to those of human in a single device is still in its infancy. In this work, a three-terminal 2D ferroelectric heterostructure consisting of α - $\text{In}_2\text{Se}_3/\text{WSe}_2$ is proposed for designing optoelectronic neuromorphic device. In contrast to conventional ferroelectric materials, the narrow bandgap of the ferroelectric α - In_2Se_3 enables the device to perceive visible light directly. Nonlinearly preprocessing is adopted by bipolar cells in the retina and computer algorithms. In the device, similar function is achieved by modulating the energy band based on ferroelectricity. The results demonstrate the ability of the device to suppress noise, and the image recognition accuracy is increased from 75% to 92%. Convolutional neural networks play an important role to extract and compress the image information for human to respond to external environment in real time. Based on the unique coupling of ferroelectricity in α - In_2Se_3 , the convolutional operation is imitated, thus allowing for reduction in image recognition time by 87%. The results provide a promising strategy to integrate diverse bio-inspired neuromorphic behaviors in a single device for artificial intelligence to process high-throughput visual information.

visual signals.^[1,2] In contrast to conventional visual information processing system, which consists of CCD cameras and computers, artificial visual systems exhibit energy-efficient manners due to the features of sensing and computing in memory. The success of artificial visual systems is primarily attributed to the imitation of the human visual system.^[3-7] The human visual system mainly involves three functions, including the perception of external visual signals, the preprocessing of visual information in the retina and the convolutional neural network (CNN) in the visual cortex of the brain for recognition and decision making. Preprocessing of images, convolutional operations for extraction and compression of image features significantly reduce the workload for the visual cortex, which makes it possible to respond in real time to high-throughput inputs of dynamic information.

Due to the tremendous application potential of artificial visual systems in the era of big data, different material systems and device structures have been

considered to design optoelectronic neuromorphic devices.^[8-14] Various neuromorphic behaviors which emulate retinal perception have also been implemented including paired-pulse facilitation (PPF), long-term potentiation (LTP), short-term

1. Introduction

Artificial visual systems refer to a hardware system which can exhibit neuromorphic behaviors in perceiving and processing

F. Guo, W. F. Io, Z. Dang, Y. Zhao, S.-Y. Pang, Y. Zhao, X. Lao, J. Hao
Department of Applied Physics
The Hong Kong Polytechnic University
Kowloon, Hong Kong 999077, P. R. China
E-mail: jh.hao@polyu.edu.hk

F. Guo, J. Hao
The Hong Kong Polytechnic University Shenzhen Research Institute
Shenzhen 518057, P. R. China
J. Hao
Photonics Research Institute and Research Institute for Smart Energy
The Hong Kong Polytechnic University
Hung Hom, Kowloon, Hong Kong 999077, P. R. China

 The ORCID identification number(s) for the author(s) of this article can be found under <https://doi.org/10.1002/aelm.202400528>

© 2024 The Author(s). Advanced Electronic Materials published by Wiley-VCH GmbH. This is an open access article under the terms of the [Creative Commons Attribution](https://creativecommons.org/licenses/by/4.0/) License, which permits use, distribution and reproduction in any medium, provided the original work is properly cited.

DOI: 10.1002/aelm.202400528

potentiation (STP), and so on.^[15–21] The implementation of preprocessing function in the retina is still in its infancy for neuromorphic devices, and most current devices increase the signal-to-noise ratio of the perceived image by repeatedly applying light pulses with different intensities based on the cumulative effect.^[22–24] Recent reports have revealed the working mechanism of preprocessing in the retina. For visual information, bipolar cells in the retina process it nonlinearly through somatic potential and neurotransmitter release.^[25,26] It effectively reduces noise and highlights the desired part of the image. However, such a function has not been explored in current neuromorphic devices. In addition, in the brain visual cortex consists of CNN, the convolutional operation is performed to compress the visual information considerably, which can reduce the workload for the back-end judgement process. Recently several proposals have been made to imitate the kernel of convolutional operations based on gate tuneable heterostructure or defect-introduced homojunction.^[27,28] By shifting the kernel, the obtained photocurrents are summed up to construct the convolutionally processed image pixels. Therefore, how to avoid the movement of the kernel for simultaneously performing the convolutional operation in parallel may be taken into consideration in future research for efficient neuromorphic computing.

Ferroelectric materials with spontaneous polarisation can provide an additional degree of freedom to functionalise the device. Conventional oxide ferroelectric materials have been investigated for decades in the fields of logic devices and memories,^[29–31] and also applied to the recent emerging neuromorphic devices as gates to modulate the conductance state of the channel.^[32,33] However, the wide bandgap and the requirement for lattice matching with the substrate limits its application in artificial visual systems for perceiving light directly. The emergence of 2D van der Waals (vdW) ferroelectric materials might bridge the gap due to their vdW contacts and semiconducting properties.^[34,35] In particular, the α - In_2Se_3 with a bandgap of ≈ 1.4 eV exhibits robust ferroelectricity even in a single atomic layer.^[36–38] The unique coupling of in-plane (IP) and out-of-plane (OOP) ferroelectricity,^[39–41] and the ability to sense visible light offer the opportunity to integrate the desired functions mentioned above in a single device.

In this work, a three-terminal ferroelectric heterojunction based on α - $\text{In}_2\text{Se}_3/\text{WSe}_2$ is proposed with elaborately selected energy band structure to integrate entire artificial visual functions including the perception of visual information, nonlinearly preprocessing and convolutional operation in a single device. The narrow bandgap of 2D ferroelectric heterostructure makes it possible to sense visible light. Nonlinearly preprocessing visual information analogous to bipolar cells is achieved through the unique coupling of IP and OOP ferroelectricity in α - In_2Se_3 to modulate the carriers in WSe_2 . Compared to the original image, the preprocessed image by our device exhibits higher contrast, and the image recognition accuracy is efficiently improved from 87% to 96%. Furthermore, the ability of the preprocessing function for noise reduction is also demonstrated. In contrast to the current approach of moving the kernel, the convolutional operation is performed in parallel after the original image is inputted into the device matrix, which greatly reduces the workload for subsequent image recognition. The results provide a new strategy to integrate preprocessing and con-

volutions analogous to that of human visual system in the optoelectronic neuromorphic device for artificial intelligence (AI) to process high-throughput visual information in the future.

2. Results and Discussion

The human visual system is composed of the retina, optical nerve, and visual cortex of brain, as illustrated in the **Figure 1a**. Perception is the first step in the workflow of the entire human visual system, where light signals from the external environment can be converted into electrical signals through the retinal cells. Beyond visual perception, the massive amount of acquired visual information will first be preprocessed in retina, which can play a significant role in highlighting the desired parts of the image and reducing noise. Besides, it also decreases the workload for the transmission of information through the optic nerve to the visual cortex in the brain. The visual cortex processes images in a convolutional method, which involves the extraction of valid information, compression of data, and recognition through neural networks. Such preprocessing and image compression abilities ensure that the human visual system can process massive amounts of real-time visual information in an energy-efficient and flexible way. **Figure 1b** is a schematic diagram of our proposed device, and the functions available in the device are demonstrated. Analogous with the human visual system, sensing, nonlinearly preprocessing and convolutional operation have been integrated at single device level based on the ferroelectric heterostructure. Cr /Au metal electrodes were initially fabricated on Si/SiO₂ substrates by standard photolithography techniques and electron-beam evaporation. Next, α - In_2Se_3 and WSe_2 nanosheets exfoliated from their bulk counterparts were placed on top of the electrodes utilizing dry transfer, which ensures excellent vdW interfaces compared to preparing electrodes on 2D materials.^[42] The narrow bandgap of α - In_2Se_3 and WSe_2 allows neuromorphic devices to sense visible light. And the unique coupling between IP and OOP ferroelectricity in 2D ferroelectric material can be modulated by the third terminal. It provides the opportunity to integrate nonlinearly preprocessing and convolutional operation functions similar to those of the human visual system into the device. Such multifunctional optoelectronic neuromorphic devices capable of perceiving visual information, preprocessing and convolutional operations shine a light for designing the future AI applications. Microscopic photo of the device is depicted in **Figure S1** (Supporting Information). There are several phases for In_2Se_3 , but only the α phase possesses coupled IP and OOP ferroelectricity due to its asymmetry of the lattice. The unique ferroelectricity originates from the movement of the central Se atom in the crystal cell. Thus, the phases of the 2D ferroelectric material were first identified by performing Raman measurements. As shown in **Figure S2** (Supporting Information), the Raman peaks are located at 88, 104, 180, and 193 cm⁻¹, respectively, and which can be attributed to E, A(LO + TO), A(TO), and A(TO) vibrational modes of the 2D ferroelectric In_2Se_3 .^[43] For α - In_2Se_3 , two different types of stacking modes have been verified, namely rhombohedral (3R) and hexagonal (2H), which belong to the space groups of R3m and P63/mmc, respectively. Although both IP and OOP ferroelectricity can be observed in them, the R3m space group exhibits more robust ferroelectricity due to aligned

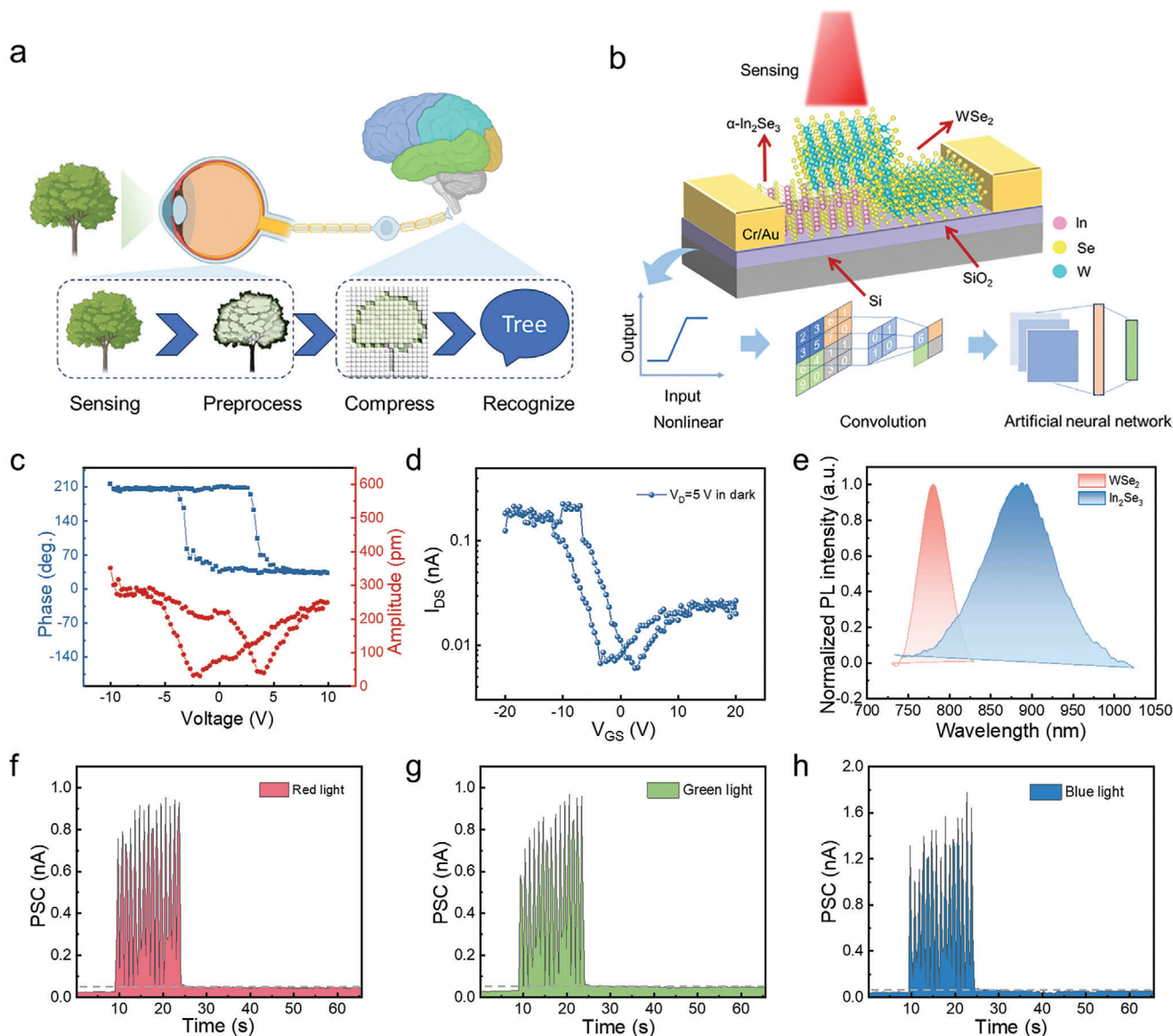


Figure 1. a) Schematic diagram of the human visual system and its functions. b) Analogous functions are integrated in our device. c) Phase and amplitude loops measurement by PFM indicate the ferroelectricity of α - In_2Se_3 . d) The transfer characteristic curve of the device where V_D is set to 5 V. e) PL spectra of WSe_2 and α - In_2Se_3 . Synaptic response with 5 V bias under f) red, g) green and h) blue light pulses of light intensity 781.6, 321.7, and 273.3 $\mu\text{W cm}^{-2}$, respectively.

stacking directions, and according to our previous research results, the crystals used in the experiments were inferred to be 3R stacking mode.^[21] Also, Raman measurements of WSe_2 were carried out, and the positions of the Raman peaks are consistent with the reported references.^[44] To investigate the ferroelectricity of α - In_2Se_3 , the nanosheets were exfoliated from the bulk and transferred to a conductive metal Pt substrate. Figure 1c shows that the phase and amplitude hysteresis loops which were obtained under dual AC resonance-tracking (DART) voltage of piezoresponse force microscopy (PFM) by a Pt/Ir-coated conductive tip. The sharp changes in parallelogram-like piezoelectric response loop and butterfly-like amplitude loop indicate that the polarity of ferroelectricity can be switched by applying voltage. The I - V

curves of p- WSe_2 /n- α - In_2Se_3 were measured under dual sweep mode from 2 V to 8 V as shown in Figure S3 (Supporting Information). The rectification behavior arises from the built-in electric field of the pn heterojunction, and the hysteresis loop is introduced by flipping the ferroelectric domains. It is a typical behavior of ferroelectric heterojunctions and illustrates the existence of IP ferroelectricity. For OOP ferroelectricity, a transfer curve was measured in the Figure 1d, the drain-source voltage (V_D) was set to 5 V, and gate voltage swept from -20 to 20 V. The butterfly-like loop demonstrates the ability of OOP ferroelectricity to modulate channel carriers. Perceiving light signals is the first task of the human visual system in acquiring and processing external information. Here, photoluminescence (PL) was carried out in

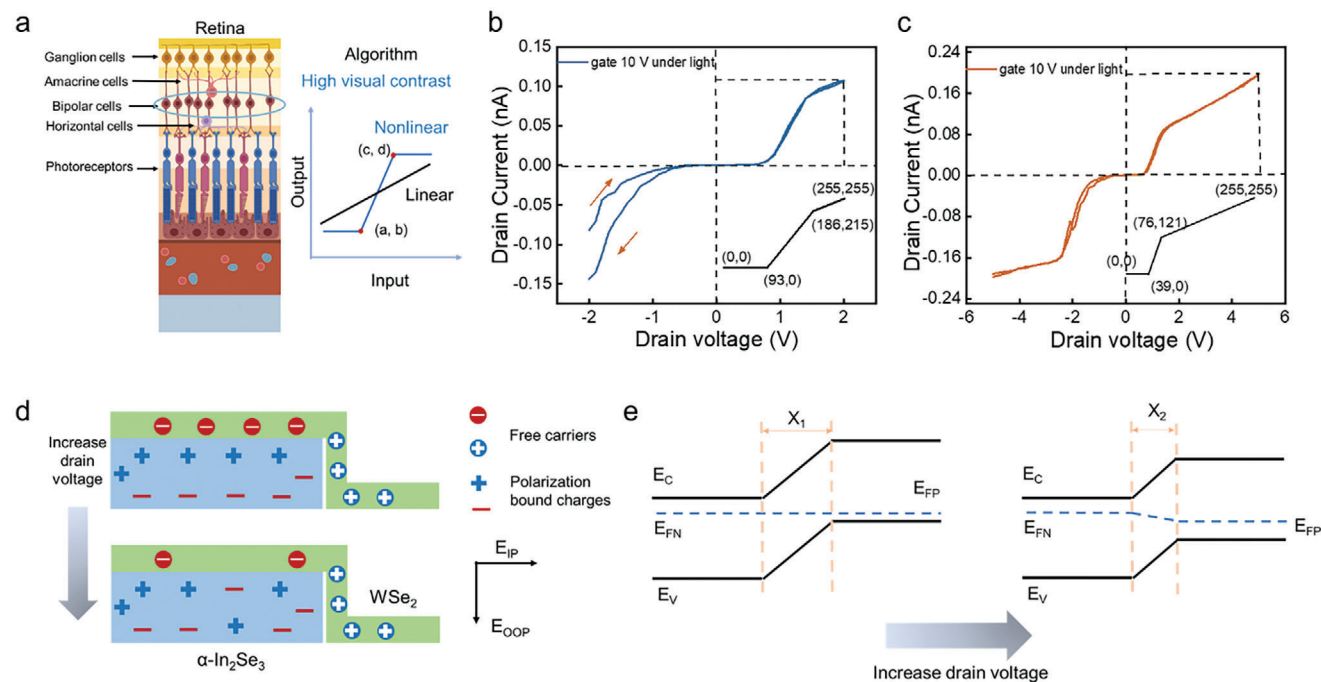


Figure 2. a) Nonlinearly preprocessing visual information is adopted by bipolar cells of the retina and software algorithms. The I - V curve of the device under gate 10 V with sweep range of b) 2 V and c) 5 V, where the drain voltage is considered as the input of the image and the current value serves as the output of the image. d) A schematic diagram depicts the distribution of carriers and bound charges in the ferroelectric heterostructure. e) The diagram shows the variation of the energy band with the drain voltage.

order to determine the sensing range of the device under 532 nm wavelength laser, as seen in the Figure 1e, the position of the PL peaks is located approximately at 780 nm and 890 nm for WSe₂ and α -In₂Se₃, respectively. It shows that our devices can perceive visible light like humans with a range from 380–780 nm. In addition, the optoelectronic synaptic behaviors of the device analogous to that of the retina are demonstrated from Figure 1f–h, where three primary colors including red, green, and blue light pulses were applied to the neuromorphic device, with light densities of 781.6, 321.7, and 273.3 $\mu\text{W cm}^{-2}$, respectively. The V_D was set as 5 V with gate voltage (V_{GS}) of 0 V. The increase in post-synaptic current (PSC) indicates the enhancement for synaptic connections and the ability of proposed device to sense visible light.

After perceiving external visual signals, the visual information which has been converted into electrical signals will be preprocessed in the retina instead of immediately transmitting to the brain visual cortex through the optical nerve. The stream of visual information flows from photoreceptors in the retina and finally reaches the terminal ganglion cells. Bipolar cells play an important role in this process for nonlinear handling of visual information, as shown in Figure 2a. Recently, Schreyer et al. reported their findings on how bipolar cells work.^[26] In contrast to previous perceptions, nonlinear processing occurs in the delivery of neurotransmitters from bipolar cells to ganglion cells. Their results suggest that the bipolar cell itself is also an independent nonlinear processing unit by changing somatic membrane potential. Nonlinear processing in bipolar cells is crucial for ganglion cells to extract image features. Also, it is a necessary step before training the artificial neural networks (ANN) for software

algorithms. In this process, the piecewise function is often used to suppress noise and improve the contrast of the image.

$$y = \begin{cases} x \times \frac{b}{a} & x < a \\ (x - a) \times \frac{d-b}{c-a} + b & a \leq x < c \\ (x - c) \times \frac{255-d}{255-c} + d & x \geq c \end{cases} \quad (1)$$

As shown in Equation (1), where y represents the output pixel brightness and x is the input pixel brightness. The (a, b) and (c, d) are the nodes of the piecewise function, which are responsible for modulating the image contrast and suppressing the magnitude of noise. However, such a function of preprocessing visual information nonlinearly has not yet been implemented in hardware neuromorphic devices. For implementing such functionality in electronic neuromorphic devices, the energy bands are carefully selected and ferroelectricity is exploited to modulate the carrier distribution in our work. Different from the electrical characteristics of conventional FETs and pn junctions, a 2D ferroelectric heterojunction with multi-level output is proposed here. Figure 2b,c depicts the I - V curves of the device with sweep ranges of 2 V and 5 V at 10 V gate bias under a 150 W halogen illuminator, respectively. The reason for performing the measurements under light is that illumination can assist the ferroelectric domains to flip more easily according to previous report.^[45] It can be seen from the figure that I - V curve shapes analogous to the piecewise function can be obtained. By changing the sweep range of the drain voltage from 2 to 5 V, the position of the nodes in the piecewise function can be modulated, thus

enabling the adjustment of the input image (Figure S4, Supporting Information). In the following part, the input drain voltage is defined as the x in the piecewise function, while the drain current is considered as y . Taking a positive drain voltage range and the typical image with a maximum pixel brightness of 255 as an example, the nodes of the piecewise function are (93, 0) and (186, 215) respectively, as shown in the inset of Figure 2b. The rectification characteristics are derived from the energy band structure of the heterostructure and the ferroelectricity in α - In_2Se_3 . Figure 2d depicts a schematic diagram of the distribution of ferroelectric bound charges and free carriers in the heterostructure. Due to the application of positive gate voltages, the direction of the polarization field of the OOP ferroelectricity is pointed downward, as a result, it induces the appearance of the inversion in WSe_2 which is placed on α - In_2Se_3 . In contrast to conventional semiconductor heterostructures, rectification generally occurs at its interfaces. In this device, the carrier transfer will be occurred through (I) the pn junction of WSe_2 caused by the modulation of the ferroelectricity, (II) the nn junction composed of WSe_2 and α - In_2Se_3 , and (III) the internal ferroelectric field in α - In_2Se_3 . According to Elad Koren et al.'s report, in which WSe_2 was placed on α - In_2Se_3 and both source-drain electrodes were prepared on WSe_2 , a similar I - V curve was obtained. Therefore, it can be deduced that (I) the WSe_2 pn junction introduced by ferroelectricity plays a major role for modulating the carrier transport in the above three regions.^[46] As demonstrated in Figure 2d,e, at low drain voltages, the reverse-biased WSe_2 pn junction hinders the movement of free carriers. With increasing the drain voltage, the electric field is enhanced, and the barrier of the heterojunction is lowered due to partial flipping of the ferroelectric domains. Eventually, when the drain voltage is further raised, current gradually saturates. Thus, a multilevel piecewise-function like I - V curve can be obtained.

According to the discussed working principle of the device, a matrix based on the extracted features from the device can be constructed and the schematic diagram is depicted in Figure 3a. All gate terminals are connected to the gate bus line. The amplitude of the drain voltage is defined as the brightness of the input pixel, while the drain current is considered as the brightness of the output one. Therefore, each neuromorphic device is available for processing an individual pixel under gate voltage, and the matrix of the device is capable of processing an image in real time. After processing by the device, the pixels are assigned new brightness in order to compose an image with high contrast and low signal-to-noise ratio. Figure 3b displays an image of a flower with 210×140 pixels that has not been processed and it is named as the original image in this work. Figure 3c shows the processed image by the device matrix, and it is observable that the noise in the background behind the flower is removed, while the spots on the petals are wiped away. And the outline of the petals and stamens become clearer with higher contrast compared to the original image. However, after treatment by the drain voltage range of 5 V, the image becomes brighter while the contrast is not improved. This is mainly attributed to the fact that the position of the second node (c, d) in the piecewise function formed by the 5 V sweep range is too low (Figure 3d). Similar phenomena can also be identified when the image is processed with other gate voltages, such as 3 and 4 V (Figure S5, Supporting Information). For comparison purpose, the pixel brightness statistics of the original image and the processed result by 2 V drain volt-

age are performed and plotted in Figure 3e. For the original image, the pixel brightness values are distributed more evenly, with the greatest distribution occurring in the 50–100 range, while the maximum value of the count stays below 5000. After processed by the drain voltage with range of 2 V, the pixel brightness distribution increases dramatically in the 0–10 interval and decreases in all other intervals. Specifically, the pixels in the low-brightness region are reduced by the largest percentage, thereby assisting with noise reduction. The statistics of pixel distribution in the processed images with other drain voltage ranges also support this trend. When the image is processed by a low drain voltage, noise can be suppressed, and the brightness distribution of the pixel becomes more uniform as the drain voltage increases (Figure S6, Supporting Information). The processed visual information can be manipulated in situ by neuromorphic devices is a promising and energy-efficient approach compared to conventional computer systems due to avoiding data transfer between separated processors and memory units. The long-term potentiation (LTP) and long-term depression (LTD) characteristics of neuromorphic devices can be achieved through the ferroelectric property in α - In_2Se_3 . As shown in Figure 3f, 25 discrete conductance states can be observed when gate voltage pulses of 10 V and a drain voltage of 5 V under light were applied continuously to the device. The negative 5 V pulse serves to reverse the OOP ferroelectric polarization, which causes the current in the channel to decrease from 0.45 to 0.41 nA. Similarly, multi-level conductance states can also be obtained by modulating the IP ferroelectricity in α - In_2Se_3 (Figure S7, Supporting Information). Compared to the conductance states introduced by IP ferroelectricity, OOP ferroelectric features illustrate better linearity and thus are extracted to construct an ANN. The ANN consists of three layers of neural network including input (x), hidden (h) and output layer (y), and the connection weights between the neural network layers are named as W_{ih} and W_{ho} , respectively (Figure 3g). The back propagation algorithm is utilized to update the weights of the neural network. After the input x is propagated forward, there is a difference between the output result y and the target value, which is defined as E . The weights are updated based on the following equation.

$$W' = W + \varphi \frac{\partial E}{\partial W} \quad (2)$$

Where W and W' represents the weight and updated weight in the neural network, and φ is the learning rate. Eventually, the E value gradually decreases below the set value and the learning process of the ANN is completed. Figure 3h depicts the results of the image recognition accuracy which improves significantly with increasing training epoch, the processed image by the 2 V I - V curve exhibits higher accuracy compared to that of original image. These results not only confirm the preprocessed images through our device can effectively improve recognition accuracy, but also demonstrate that the ANN consisting of the device is capable of processing perceived visual signals in situ.

Noise is inevitable when perceiving visual information for practical applications of artificial visual systems. The diversity of noise sources can be induced during the stage of perception of visual signals or from the interference of high-speed electrical signals when processing image. Figure 4a is a side-view schematic

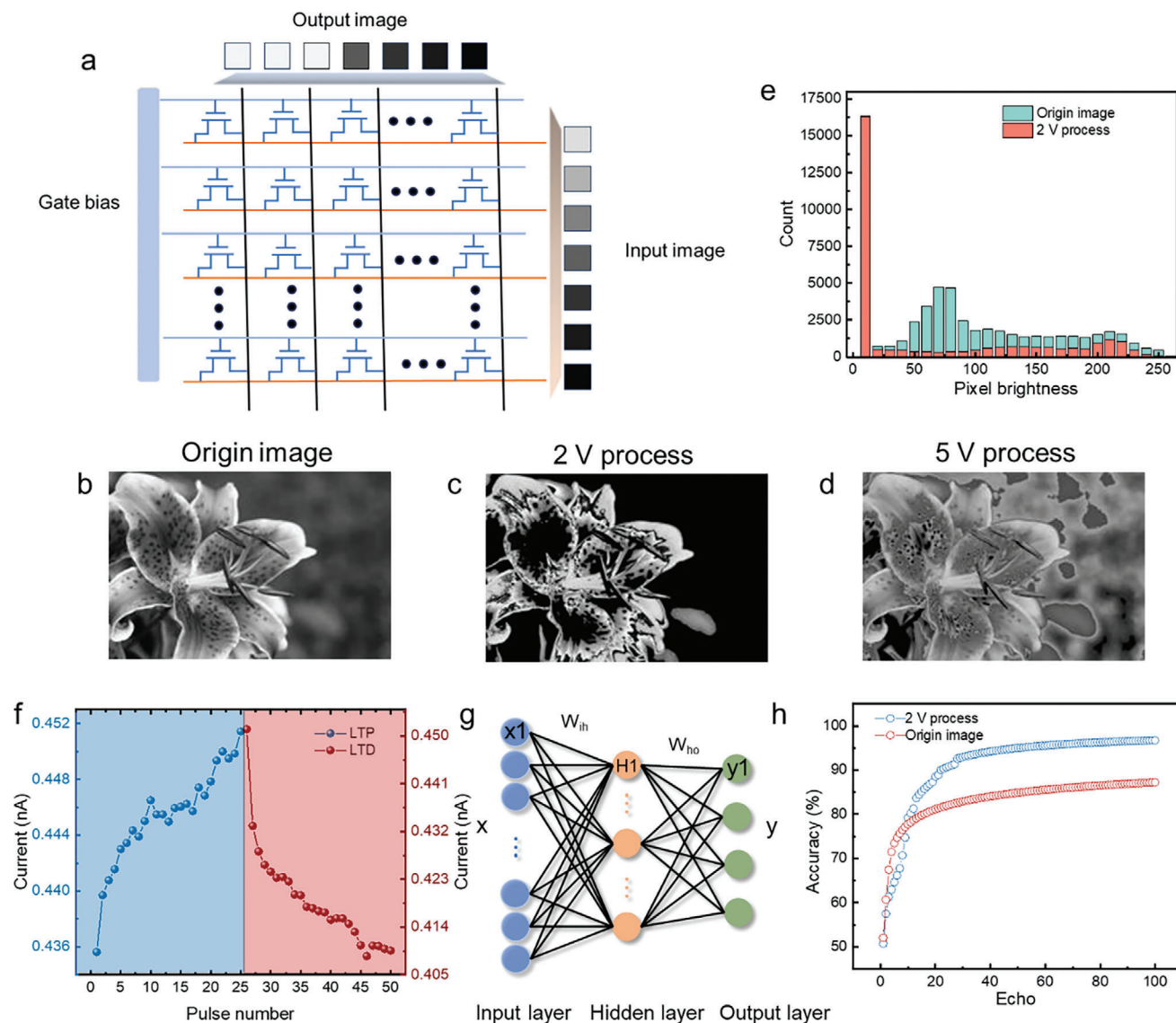


Figure 3. a) Working principle of device matrix to preprocess the image. b) The original image and the processed ones via c) 2 V and d) 5 V I - V curves for comparison. e) Redistributed pixels of the original image and the image after preprocessing. f) Controllable conductance states are obtained by applying gate pulses of 10 V and -5 V respectively with 5 V drain voltage. g) A three-layer ANN is built for recognizing images. h) The preprocessed image exhibits higher recognition accuracy with the increasing training echo as compared to the original image.

diagram of the device structure, with the help from IP or OOP ferroelectricity in α - In_2Se_3 , electrical pulses from the gate or the drain terminals can be applied to the neuromorphic device to create noise in the perceived image for the purpose of verifying the performance of the device. Salt-and-pepper noise, also termed as impulse noise, is commonly seen in digital images with abrupt white or black spots, which may be caused by pixel damage or strong interference. The original image with salt-and-pepper noise is shown in Figure 4b. Identical to the treatment in Figure 3c, each pixel is processed by a piecewise function consisting of the 2 V I - V curve, and the output image can be seen in Figure 4c. Fewer noise pixels and sharper outlines are clearly observable compared to the unprocessed image. Figure 4d,e depicts the statistic results of the original image with noise and the

image processed by our device respectively. The brightness of the pixels in the original image with noise is more distributed in the middle region, while the number of pixels around the value of 100 is the maximum exceeding 6000 counts. On the contrary, the pixels of the processed image are mainly concentrated in regions with low brightness values, in which the number of pixels with a brightness value of about ten can reach up to 16 000. The increase of image recognition accuracy from 75% to 92% shown in Figure 4f also proves the capability of the device for improving the quality of images with noise.

The preprocessed visual information is passed through the optic nerve to the visual cortex of the brain and manipulated via a CNN located there. The CNN of the human brain can perform a similar function to the convolution of mathematics. In the front

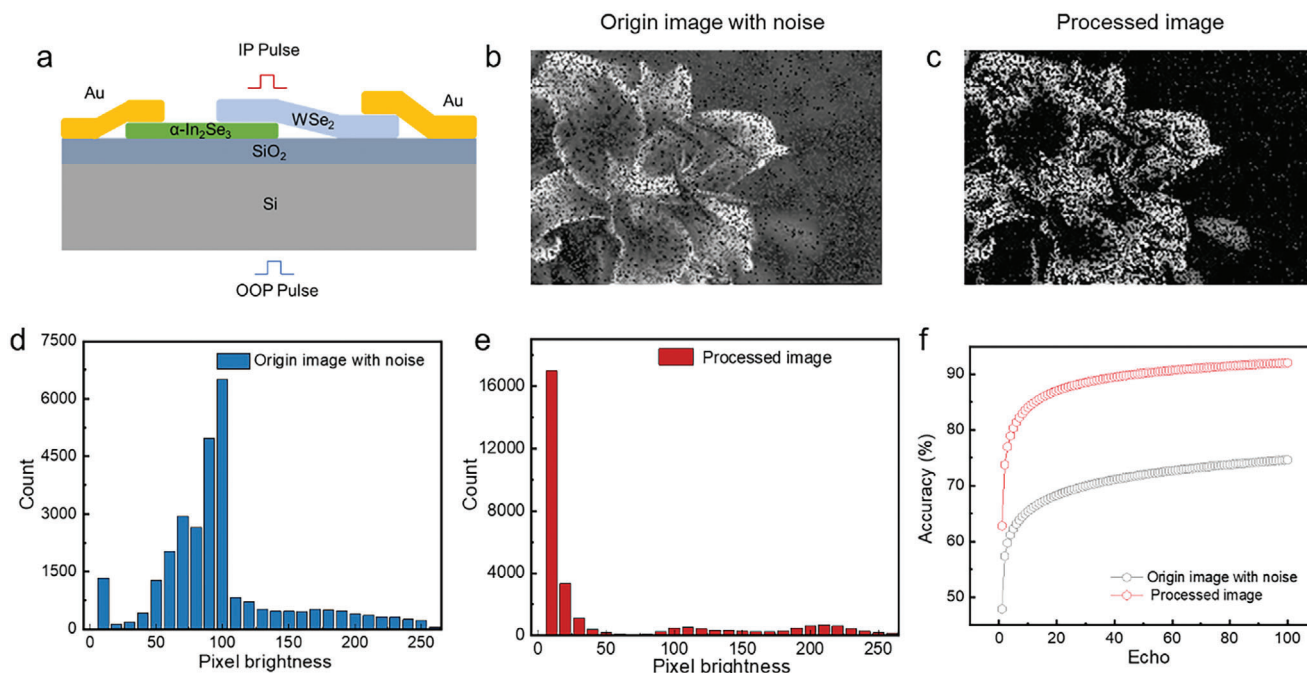


Figure 4. a) Schematic diagram of a three-terminal neuromorphic device, where Si serves as gate for flipping the OOP ferroelectricity, source, and drain are employed to modulate the IP ferroelectricity. b) Salt and pepper noise has been added to the original image. c) Image with noise is processed nonlinearly. d) The pixel brightness of the original image with noise is compared to e) the processed image. f) The processed image exhibits higher recognition accuracy.

part of the neural network, the features of the image will be extracted and compressed, and the compressed visual information will then be sent to the neural network for recognition. Such a process effectively reduces the workload of the image recognition neural network, so that the brain can rapidly make appropriate judgements and responses to the dynamic visual information from the external world in real time. Due to the efficient behavior of CNN for processing visual information, the method has also been imitated and adopted in software algorithms. However, how to implement CNN in neuromorphic devices still remains a challenge. Recently, several device structures have been proposed to mimic the function of kernel in CNN. Convolutional operations are carried out by constantly perceiving the illuminated image and moving the kernel based on a matrix of devices, typically 3×3 or 5×5 , time after time. Then, the photocurrents perceived each time as pixels recompose a desired image. Here, an electrically convolutional operation working mode in parallel manner is proposed based on the unique IP and OOP ferroelectricity in our ferroelectric heterostructure. **Figure 5a** depicts the input of the perceived visual image into the device matrix, where each device represents one pixel and the whole device matrix can display the entire image by setting different conductance states. For our device, 16 ascending conductance states induced by reversing IP ferroelectricity when applying drain voltage are served as 16 different pixel brightness, as shown in **Figure 5b**. When the image is fed into the device matrix, the conductance states of all the devices are updated in parallel from the first electrical pulse up to the sixteenth, the working principle is consistent with the process of updating the weights in an ANN crossbar. The process of visual image input into the device matrix is displayed in **Figure 5c**.

After applying 5 electrical pulses, the outline of the flower is gradually revealed and the details in the flower can be observed when 16 electrical pulses are applied. In order to investigate the performance of the device, the nonlinearity during the updating conductance state is also taken into consideration. Compared to the flower image, which is fed through 16 electrical pulses with perfect linearity (**Figure S8**, Supporting Information), there is only slight noise that appears in the image introduced by the electrical pulses. After the image is input into the device matrix, a convolutional operation is performed to compress the size of the image. The kernel of the convolutional operation consists of 3×3 elements, where the surrounding element 0 is represented by the applied gate terminal voltage and the center 1 is not. As shown in the **Figure 5b**, the OOP electrical pulse can effectively reset the conductance state of the channel to the lowest level which is considered as 0. The gate voltage is chosen to emulate the kernel for the reason of the coupling between the OOP and IP ferroelectricity. Moreover, the switching voltage of the OOP ferroelectric polarization is only one-tenth as much as that of its IP ferroelectricity, making it a much more effective way to modulate the channel conductance state introduced by the IP ferroelectricity.^[39] **Figure 5d** shows the principle of the convolution process, where stride is defined as the distance between two kernels, which can be used to control the compression ratio of the image. Different from the previously proposed method of moving the kernels, for our device matrix, applying gate voltage pulses in parallel allows the convolutional operation to be performed simultaneously. The original image is compressed through different magnitudes of stride and the image can be resized from 29 400 to 1820 pixels as shown in the **Figure 5e**. For demonstrating

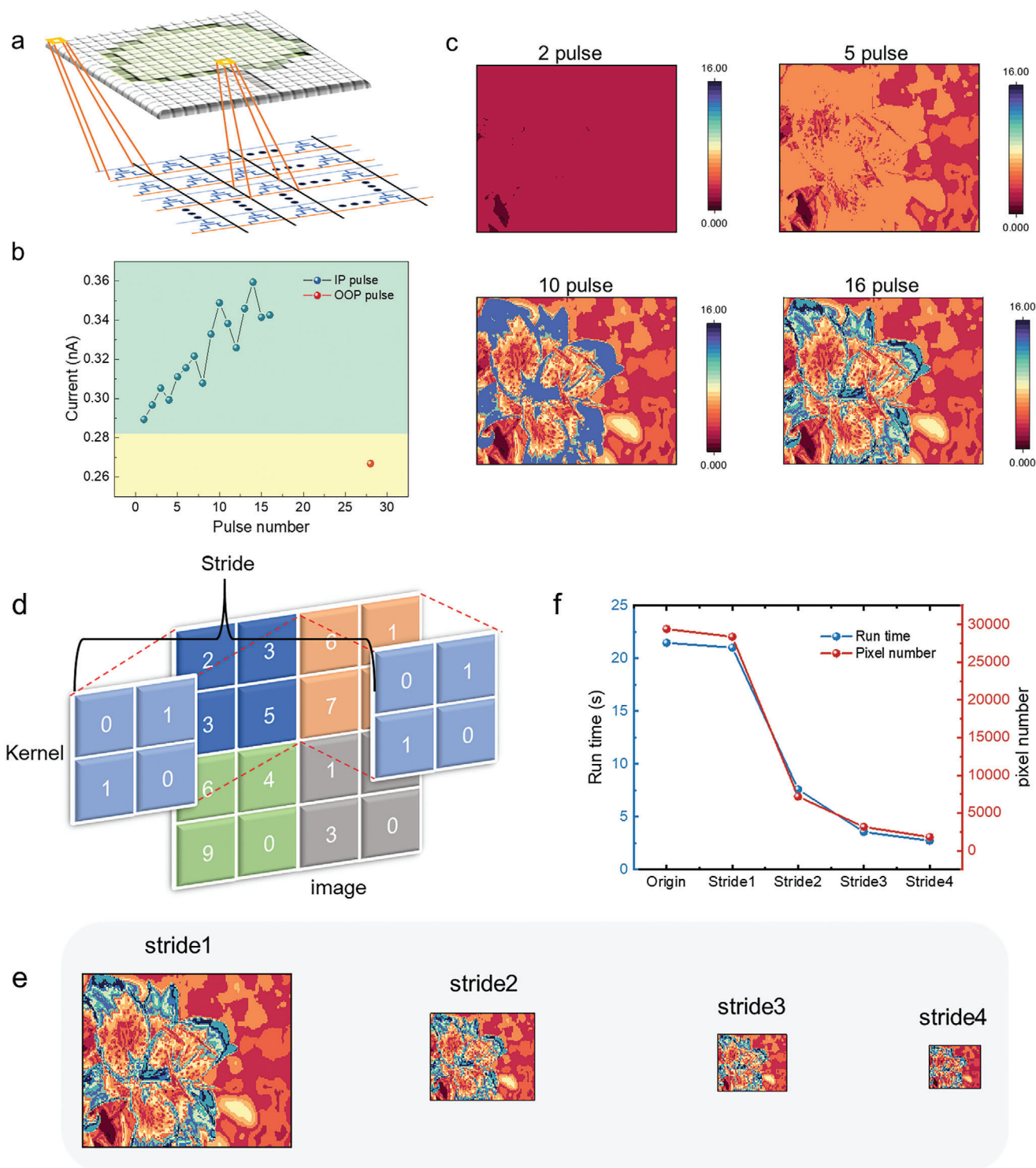


Figure 5. a) The image is input into a device matrix, each device is considered as a pixel. b) Conductance states introduced by IP ferroelectricity are employed to construct the image, and OOP ferroelectric modulation plays a role to emulate the kernel. c) The image to be input into the device matrix becomes gradually clearer with increasing IP electrical pulses. d) Principle of convolutional operation. e) When the stride of the kernel is increased, the image size is compressed and the number of pixels is reduced. f) The results show that the time required to recognize the image decreases as the image is compressed.

how convolutional operations improve the efficiency of image recognition, the time required to process 100 training echoes is evaluated. After 100 training echoes, there is no significant difference in image recognition accuracy, and they are all >90% in the case of different stride. The statistic results in Figure 5f show that as the image size is compressed, the time employed to train an ANN to recognize the image can be greatly reduced from 21.5 to 2.7 s.

3. Conclusion

In conclusion, a three-terminal optoelectronic neuromorphic device is proposed based on 2D ferroelectric heterostructure α - $\text{In}_2\text{Se}_3/\text{WSe}_2$, where the entire functions of the human visual system including perception, nonlinear preprocessing and convolutional operation are integrated in a single device. Sensing visible light in devices is attributed to the bandgap structure of the α - In_2Se_3 and WSe_2 . Importantly, nonlinearly preprocessing images analogous to the human retina and computer algorithms is achieved in a neuromorphic device by the effect of ferroelectricity on free carriers in heterostructure. Consequently, the noise can be suppressed, the contrast of the image is improved, and the image recognition accuracy is raised from 75% to 92%. In addition, the IP ferroelectricity is exploited to input the image into the device matrix and the OOP ferroelectricity serves to imitate the kernel. Successful emulation of convolutional operation in a parallel manner which avoids kernel movement can considerably improve the efficiency of image processing. Our work takes a further step toward implementing human visual system inspired functions in neuromorphic devices for AI to flexibly process visual information in real time.

4. Experimental Section

Device Fabrication: Au/Cr electrodes (30 nm/10 nm) were prepared on Si substrates with SiO_2 (290 nm) by a standard lithography technique and electron-beam evaporation. The α - In_2Se_3 and WSe_2 crystals were purchased from the HQ Graphene company and their nanosheets were obtained by a mechanical exfoliation method using scotch tape. The nanosheets were transferred on PDMS film which was fixed on a glass slide and then placed on dry transfer platform. The microscope of the dry transfer platform was applied to align the nanosheets and electrodes. Finally, under 60 °C, the nanosheets were detached from the PDMS and heterostructures were prepared.

Characterizations: Phase and amplitude hysteresis loops were obtained to verify ferroelectricity of α - In_2Se_3 via the Asylum MFP 3D Infinity system. Raman and PL spectra measurements were carried out by utilizing the WITec-Confocal Raman system equipped with a 532 nm laser. Light pulses were realized through LEDs with different wavelengths, which were calibrated by a Sanwa optical power meter. Electrical characteristics were measured by a semiconductor analyzer Keithley 4200-SCS. The code is written in python and based on the CrossSim platform which run in integrated development environment Spyder.^[47]

Supporting Information

Supporting Information is available from the Wiley Online Library or from the author.

Acknowledgements

This work was supported by grants from the National Natural Science Foundation of China (No. 52233014), the Research Grants Council of Hong Kong (SRFS 2122-5S02), the HKPFS (Ref. No. PF20-46080), and the PolyU Grants (1-CE0H, 1-W22S, and 1-CD7V).

Conflict of Interest

The authors declare no conflict of interest.

Data Availability Statement

The data that support the findings of this study are available from the corresponding author upon reasonable request.

Keywords

2D van der Waals material, α - $\text{In}_2\text{Se}_3/\text{WSe}_2$, ferroelectric heterostructure, optoelectronic neuromorphic device

Received: July 23, 2024

Revised: August 27, 2024

Published online:

- [1] Y. Sun, S. Xu, Z. Xu, J. Tian, M. Bai, Z. Qi, Y. Niu, H. H. Aung, X. Xiong, J. Han, C. Lu, J. Yin, S. Wang, Q. Chen, R. Tenne, A. Zak, Y. Guo, *Nat. Commun.* **2022**, *13*, 5391.
- [2] W. Qiu, Y. Huang, L. A. Kong, Y. Chen, W. Liu, Z. Wang, J. Sun, Q. Wan, J. H. Cho, J. Yang, Y. Gao, *Adv. Funct. Mater.* **2020**, *30*, 2002325.
- [3] F. Liao, Z. Zhou, B. J. Kim, J. Chen, J. Wang, T. Wan, Y. Zhou, A. T. Hoang, C. Wang, J. Kang, J.-H. Ahn, Y. Chai, *Nat. Electron.* **2022**, *5*, 84.
- [4] J. Yu, Y. Wang, S. Qin, G. Gao, C. Xu, Z. L. Wang, Q. Sun, *Mater. Today* **2022**, *60*, 158.
- [5] J. K. Han, M. Kang, J. Jeong, I. Cho, J. M. Yu, K. J. Yoon, I. Park, Y. K. Choi, *Adv. Sci.* **2022**, *9*, 2106017.
- [6] Y. Hu, H. Yang, J. Huang, X. Zhang, B. Tan, H. Shang, S. Zhang, W. Feng, J. Zhu, J. Zhang, Y. Shuai, D. Jia, Y. Zhou, P. Hu, *ACS Appl. Mater. Interfaces* **2022**, *14*, 55839.
- [7] X. Li, S. Li, B. Tang, J. Liao, Q. Chen, *Adv. Electron. Mater.* **2022**, *8*, 2200343.
- [8] X. Wang, Y. Zong, D. Liu, J. Yang, Z. Wei, *Adv. Funct. Mater.* **2023**, *33*, 2213894.
- [9] X. Chen, Y. Xue, Y. Sun, J. Shen, S. Song, M. Zhu, Z. Song, Z. Cheng, P. Zhou, *Adv. Mater.* **2023**, *35*, 2203909.
- [10] Y.-X. Hou, Y. Li, Z.-C. Zhang, J.-Q. Li, D.-H. Qi, X.-D. Chen, J.-J. Wang, B.-W. Yao, M.-X. Yu, T.-B. Lu, J. Zhang, *ACS Nano* **2020**, *15*, 1497.
- [11] X. Shan, C. Zhao, X. Wang, Z. Wang, S. Fu, Y. Lin, T. Zeng, X. Zhao, H. Xu, X. Zhang, Y. Liu, *Adv. Sci.* **2022**, *9*, 2104632.
- [12] Q. Li, T. Wang, Y. Fang, X. Hu, C. Tang, X. Wu, H. Zhu, L. Ji, Q.-Q. Sun, D. W. Zhang, L. Chen, *Nano Lett.* **2022**, *22*, 6435.
- [13] K. Liao, P. Lei, M. Tu, S. Luo, T. Jiang, W. Jie, J. Hao, *ACS Appl. Mater. Interfaces* **2021**, *13*, 32606.
- [14] G. Bai, Y. Lyu, Z. Wu, S. Xu, J. Hao, *Sci. China Mater.* **2020**, *63*, 575.
- [15] R. Ji, G. Feng, C. Jiang, B. Tian, C. Luo, H. Lin, X. Tang, H. Peng, C. G. Duan, *Adv. Electron. Mater.* **2022**, *8*, 2101402.
- [16] M. Xu, X. Mai, J. Lin, W. Zhang, Y. Li, Y. He, H. Tong, X. Hou, P. Zhou, X. Miao, *Adv. Funct. Mater.* **2020**, *30*, 2003419.
- [17] W. Huang, P. Hang, Y. Wang, K. Wang, S. Han, Z. Chen, W. Peng, Y. Zhu, M. Xu, Y. Zhang, Y. Fang, X. Yu, D. Yang, X. Pi, *Nano Energy* **2020**, *73*, 104790.

- [18] C. Zhu, H. Liu, W. Wang, L. Xiang, J. Jiang, Q. Shuai, X. Yang, T. Zhang, B. Zheng, H. Wang, D. Li, A. Pan, *Light: Sci. Appl.* **2022**, *11*, 337.
- [19] G. Zhou, J. Li, Q. Song, L. Wang, Z. Ren, B. Sun, X. Hu, W. Wang, G. Xu, X. Chen, L. Cheng, F. Zhou, S. Duan, *Nat. Commun.* **2023**, *14*, 8489.
- [20] K. Wang, Y. Jia, X. Yan, *Adv. Funct. Mater.* **2021**, *31*, 2104304.
- [21] F. Guo, M. Song, M. C. Wong, R. Ding, W. F. Io, S. Y. Pang, W. Jie, J. Hao, *Adv. Funct. Mater.* **2022**, *32*, 2108014.
- [22] N. Yantara, S. E. Ng, D. Sharma, B. Zhou, P. S. V. Sun, H. M. Chua, N. F. Jamaludin, A. Basu, N. Mathews, *Adv. Mater.* **2024**, *36*, 2305857.
- [23] J. Meng, T. Wang, H. Zhu, L. Ji, W. Bao, P. Zhou, L. Chen, Q.-Q. Sun, D. W. Zhang, *Nano Lett.* **2021**, *22*, 81.
- [24] Z. Dang, F. Guo, Y. Zhao, K. Jin, W. Jie, J. Hao, *Adv. Funct. Mater.* **2024**, *34*, 2400105.
- [25] S. P. Kuo, G. W. Schwartz, F. Rieke, *Neuron* **2016**, *90*, 320.
- [26] H. M. Schreyer, T. Gollisch, *Neuron* **2021**, *109*, 1692.
- [27] T. Li, J. Miao, X. Fu, B. Song, B. Cai, X. Ge, X. Zhou, P. Zhou, X. Wang, D. Jariwala, W. Hu, *Nat. Nanotechnol.* **2023**, *18*, 1303.
- [28] L. Pi, P. Wang, S.-J. Liang, P. Luo, H. Wang, D. Li, Z. Li, P. Chen, X. Zhou, F. Miao, T. Zhai, *Nat. Electron.* **2022**, *5*, 248.
- [29] W. Banerjee, A. Kashir, S. Kamba, *Small* **2022**, *18*, 2107575.
- [30] I. J. Kim, J. S. Lee, *Adv. Mater.* **2023**, *35*, 2206864.
- [31] S. Yuan, Z. Yang, C. Xie, F. Yan, J. Dai, S. P. Lau, H. Chan, J. Hao, *Adv. Mater.* **2016**, *28*, 10048.
- [32] J. Li, C. Ge, J. Du, C. Wang, G. Yang, K. Jin, *Adv. Mater.* **2020**, *32*, 1905764.
- [33] J. Chen, X.-C. Zhao, Y.-Q. Zhu, Z.-H. Wang, Z. Zhang, M.-Y. Sun, S. Wang, Y. Zhang, L. Han, X.-M. Wu, T.-L. Ren, *ACS Nano* **2023**, *18*, 581.
- [34] Z. Guan, H. Hu, X. Shen, P. Xiang, N. Zhong, J. Chu, C. Duan, *Adv. Electron. Mater.* **2020**, *6*, 1900818.
- [35] L. Qi, S. Ruan, Y. J. Zeng, *Adv. Mater.* **2021**, *33*, 2005098.
- [36] Y. T. Huang, N. K. Chen, Z. Z. Li, X. P. Wang, H. B. Sun, S. Zhang, X. B. Li, *InfoMat* **2022**, *4*, e12341.
- [37] L. Wang, X. Wang, Y. Zhang, R. Li, T. Ma, K. Leng, Z. Chen, I. Abdelwahab, K. P. Loh, *Adv. Funct. Mater.* **2020**, *30*, 2004609.
- [38] W. F. Io, S. Yuan, S. Y. Pang, L. W. Wong, J. Zhao, J. Hao, *Nano Res.* **2020**, *13*, 1897.
- [39] W. Ding, J. Zhu, Z. Wang, Y. Gao, D. Xiao, Y. Gu, Z. Zhang, W. Zhu, *Nat. Commun.* **2017**, *8*, 14956.
- [40] F. Xue, X. He, Y. Ma, D. Zheng, C. Zhang, L.-J. Li, J.-H. He, B. Yu, X. Zhang, *Nat. Commun.* **2021**, *12*, 7291.
- [41] F. Guo, W. F. Io, Z. Dang, R. Ding, S.-Y. Pang, Y. Zhao, J. Hao, *Mater. Horiz.* **2023**, *10*, 3719.
- [42] Y. Liu, J. Guo, E. Zhu, L. Liao, S.-J. Lee, M. Ding, I. Shakir, V. Gambin, Y. Huang, X. Duan, *Nature* **2018**, *557*, 696.
- [43] Y. Zhou, D. Wu, Y. Zhu, Y. Cho, Q. He, X. Yang, K. Herrera, Z. Chu, Y. Han, M. C. Downer, H. Peng, K. Lai, *Nano Lett.* **2017**, *17*, 5508.
- [44] E. Del Corro, H. Terrones, A. Elias, C. Fantini, S. Feng, M. A. Nguyen, T. E. Mallouk, M. Terrones, M. A. Pimenta, *ACS Nano* **2014**, *8*, 9629.
- [45] F. Xue, X. He, W. Liu, D. Periyangounder, C. Zhang, M. Chen, C. H. Lin, L. Luo, E. Yengel, V. Tung, T. D. Anthopoulos, L.-J. Li, J.-H. He, X. Zhang, *Adv. Funct. Mater.* **2020**, *30*, 2004206.
- [46] M. Uzhansky, S. Mukherjee, G. Vijayan, E. Koren, *Adv. Funct. Mater.* **2024**, *34*, 2306682.
- [47] E. J. Fuller, F. E. Gabaly, F. Léonard, S. Agarwal, S. J. Plimpton, R. B. Jacobs-Gedrim, C. D. James, M. J. Marinella, A. A. Talin, *Adv. Mater.* **2016**, *29*, 0935.